# Cooccurrence of Fe-, Fe-Ca-, and Ca-Phosphate Minerals in Concretions Within the Monterey Formation: A Record of Uplift of the Santa Maria Basin, California

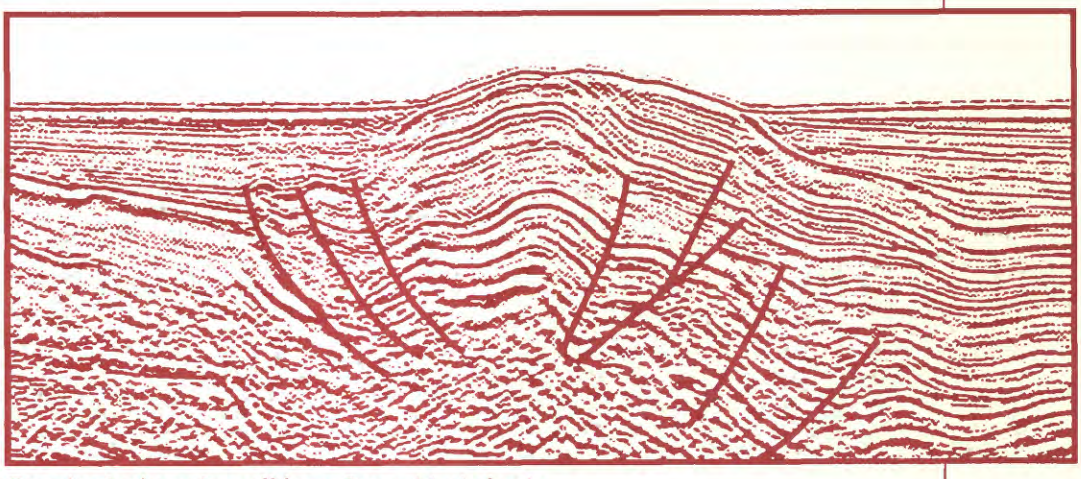

Geophysical section offshore Santa Maria basin

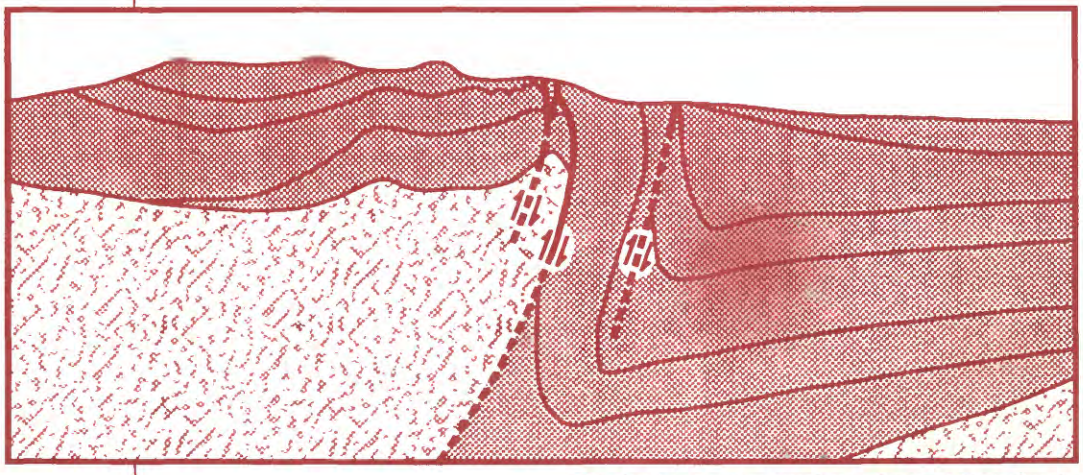

Geologic section onshore Santa Maria basin

U.S. GEOLOGICAL SURVEY BULLETIN 1995–C

## COVER

TOP—Seismic-reflection profile at approximately 350-m water depth through the Queenie structure in the offshore Santa Maria Basin. Section shown here, from line 812, was processed by Patrick H. McClellan. This profile is part of a larger set of seismic data collected in the offshore Santa Maria Basin during 1978 by the U.S. Geological Survey research vessel *Samuel P. Lee.*

BOTTOM—Northeast-southwest cross section through the Casmalia Hills and Santa Maria Valley areas of the onshore Santa Maria Basin, modified slightly from Woodring and Bramlette (1950). The Cretaceous, Tertiary, and Quaternary sedimentary sequence overlies igneous and metamorphic rocks of Mesozoic age.

Chapter C

# Cooccurrence of Fe-, Fe-Ca-, and Ca-Phosphate Minerals in Concretions Within the Monterey Formation: A Record of Uplift of the Santa Maria Basin, California

By D.Z. PIPER, C.M. ISAACS, and M.D. MEDRANO

U.S. GEOLOGICAL SURVEY BULLETIN 1995

EVOLUTION OF SEDIMENTARY BASINS/ONSHORE OIL AND GAS INVESTIGATIONS—
SANTA MARIA PROVINCE

Edited by Margaret A. Keller

U.S. DEPARTMENT OF THE INTERIOR
BRUCE BABBITT, Secretary

U.S. GEOLOGICAL SURVEY
Dallas L. Peck, Director

Any use of trade, product, or firm names
in this publication is for descriptive purposes only
and does not imply endorsement by the U.S. Government

Text and illustrations edited by George A. Havach

UNITED STATES GOVERNMENT PRINTING OFFICE, WASHINGTON : 1993

For sale by
Book and Open-File Report Sales
U.S. Geological Survey
Federal Center, Box 25286
Denver, CO 80225

**Library of Congress Cataloging in Publication Data**

Piper, David Z.
Cooccurrence of Fe-, Fe-Ca-, and Ca-phosphate minerals in concretions within the Monterey Formation : a record of uplift of the Santa Maria Basin, California / by D.Z. Piper, C.M. Isaacs, and M.D. Medrano.
p. cm.—(Evolution of sedimentary basins—Santa Maria Province ; ch. C) (U.S. Geological Survey bulletin ; 1995)
Includes bibliographical references.
Supt. of Docs. no. : I 19.3:1995C
1. Phosphate minerals—California—Lompoc Region. 2. Geology, Stratigraphic—Miocene. 3. Geology—California—Lompoc Region. 4. Monterey Formation (Calif.) I. Isaacs, Caroline M. II. Medrano, M.D. III. Title. IV. Title: Co-occurrence of Fe-, Fe-Ca-, and Ca-phosphate minerals in concretions within the Monterey Formation. V. Series. VI. Series: U.S. Geological Survey bulletin; 1995-C.
QE75.B9 no. 1995-C
[QE389.64]
557.3 s—dc20
[553.6'4'0979491]

92-28029
CIP

# CONTENTS



## FIGURES



## TABLES

# Cooccurrence of Fe-, Fe-Ca-, and Ca-Phosphate Minerals in Concretions Within the Monterey Formation: A Record of Uplift of the Santa Maria Basin, California

*By* D.Z. Piper, C.M. Isaacs, *and* M.D. Medrano

**Abstract**

Phosphatic concretions occur within diatomite in the upper part of the Miocene Monterey Formation near Lompoc, Calif. Absence of disruption of fine laminar bedding in the associated sediment by the concretions shows that they formed after complete compaction of the enclosing sediment.

The concretions exhibit a strongly concentric color, chemical, and mineralogic zonation. Many of them are composed of a nucleus in which vivianite is the dominant mineral. Amorphous ferric phosphate, mitridatite, and francolite are the dominant phosphatic phases in successive layers toward the surface of the concretions. Cd and As contents increase tenfold from the nucleus outward, reaching a maximum of 2,000 ppm, whereas Ni content, with a maximum of 720 ppm, and Co content show the opposite trend.

This mineralogy and elemental composition favor accretion under conditions of continuously increasing Eh and pH, during uplift into the fresh-ground-water zone of the terrestrial environment. Shale-normalized rare-earth-element patterns, however, suggest a marine source for the elements—biogenic debris consisting of opal-A, organic matter, and carbonates of the enclosing sediment.

## INTRODUCTION

Concretions recovered from marine sedimentary rocks can range in size from a few tenths of a millimeter to several tens of centimeters across. The structural relation of the enclosing sediment to the concretions, as viewed in outcrop, can reveal the timing of their precipitation: (1) under marine conditions—at the sediment surface during deposition, at a shallow depth of burial during early diagenesis, or at a late stage of burial and diagenesis after compaction of the enclosing sediment—or (2) under fresh-ground-water conditions—during uplift into the terrestrial environment.

Manuscript approved for publication, May 26, 1992.

Their composition and mineralogy reflect the chemistry of the water within which they formed. For example, ferromanganese nodules occur within pelagic marine sediment (Elderfield and others, 1981) under relatively high Eh and pH conditions, whereas concretions composed of vivianite require reducing freshwater conditions of approximately neutral pH (Hearn and others, 1983). Other mineralogies for concretions in sedimentary rocks include silica (opal-CT and quartz), carbonates (calcite, manganocalcite, dolomite, and siderite), hydroxide (bauxite), oxides (todorokite, $\delta$-$MnO_2$, and goethite) and sulfides (pyrite), to name but a few, which reflect still other water chemistries.

In this study, we examine the mineralogy and chemical composition of phosphate concretions collected from the Monterey Formation at the Celite (formerly Johns Manville) mine, a diatomite quarry located 5 km south of the city of Lompoc, Calif. (fig. 1). The diatomite is thinly laminated (fig. 2) and consists of as much as 95 weight percent biogenic silica. Whereas concretions at other localities of this formation are composed predominantly of silica, calcite, dolomite, and (or) francolite (Bramlette, 1946; Murata and others, 1969, 1972; Pisciotto, 1981), those examined here have a unique mineralogy. In one concretion, the dominant phases in successive envelopes from the nucleus to the outer surface are vivianite, amorphous ferric phosphate, mitridatite, and francolite; in another concretion, precipitation of an Mn-Ni-Zn oxide followed that of francolite.

We interpret this complex mineralogy of phosphate and oxide phases and their chemical and structural relations to the host sediment in terms of the sequence of chemical changes that controlled the composition of the concretions and the approximate timing of their formation.

*Acknowledgments.*—Reviews of the manuscript were generously provided by R. Koski, W. Carothers, and G. McClellan. The X-ray-fluorescence and inductively coupled plasma emission-spectroscopic analyses were carried out at the U.S. Geological Survey's laboratory in Denver, Colo. R. Erd provided X-ray-diffraction analyses. The personnel at the Celite mine provided us access to the site and several of the concretions examined.

## ANALYTICAL TECHNIQUES

The concretions were analyzed for mineralogy by X-ray diffraction (XRD); for major-element oxides by X-ray fluorescence (XRF), inductively coupled plasma optical-emission spectroscopy (ICP–OES), XRF scanning-electron microscopy (XRF–SEM), and microprobe; and for minor elements by ICP–OES. The precision of the XRF and ICP analyses, which is better than 10 percent for all analyses, has been established by repeated analyses of U.S. Geological Survey rock and ore standards over several decades (Crock and Lichte, 1982; Lichte and others, 1987; Taggart and others, 1987), as well as by concurrent analyses. The precision of the microprobe analyses is better than 7 percent, as determined by our analyses of 10 rock and ore standards. The precision of microprobe fluo-

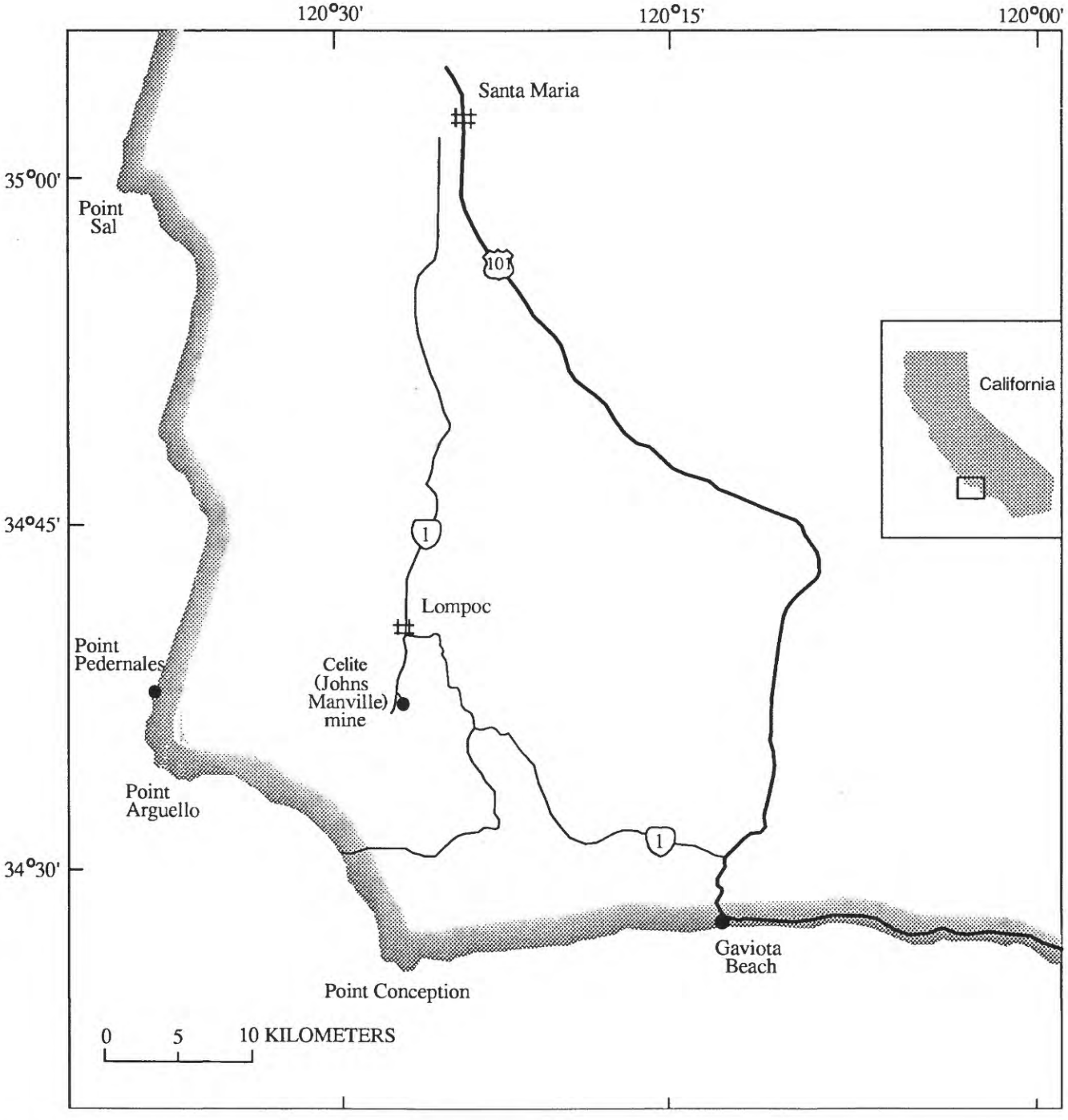


**Figure 1.** Index map of California, showing location of the Celite mine.

rine analyses, however, is poorer than 10 percent at F contents less than about 1.5 weight percent, and poorer than 50 percent at F contents less than about 0.3 weight percent. ICP–OES analyses of sample aliquants for minor elements showed less reproducibility than the approximately 15-percent precision of earlier studies, except for rare-earth elements (REE's). This apparent loss in precision likely reflects sample heterogeneities, rather than larger analytical errors.

Total carbon and organic carbon were measured by an induction-furnace carbon analyzer; precision is better than 10 percent. Analyses of calcite-spiked samples have a precision of 5 percent.

## RESULTS

The concretions occur within an approximately 50-m-thick section of the Monterey Formation (upper Miocene). They are spherical to lenticular and 1 to 6 cm in diameter. Polished surfaces exhibit a concentric color zonation. In concretion 5–1 (fig. 3), layer 1, the outermost envelope, is white to olive yellow (5Y6/6); layer 2 is grayish olive (10Y4/2); layer 3 is light olive brown (5Y5/6); layer 4 is moderate reddish brown (10R4/6) but with a well-defined, 1-mm-thick, dusky-red (10R3/6) zone at its outer edge; and layer 5, the nucleus, is dusky blue (5PB3/2). Visually, part of the nucleus changes color on exposure to resemble layer 3. Under transmitted light, the phosphatic matrix in layer 1 is colorless; in layers 2, 3, and 4 it is deep red; and in layer 5 it is blue and, where microcrystalline, strongly pleochroic; it remains so even after exposure to air.

Most of the concretions examined in the field consist of two to four layers; a dusky-blue nucleus is absent. Many concretions enclose interiors filled with friable diatomaceous silica (concretions 6–A, 6–B, fig. 3), but none contain an identifiable nucleating solid phase.

### Major-Element Oxides

The major-element-oxide composition of the five layers in concretion 5–1 (table 1) strongly reflects the color differences of individual layers. CaO decreases in content from 23.2 weight percent in layer 1 to 2.4 weight percent in layer 5, whereas $Fe_2O_3$ (considered to be present as $Fe^{2+}$ in layer 5, owing to its mineralogy; see below) shows the opposite trend. The F content exceeds 0.2 weight percent only in layers 1 and 2, and inorganic $CO_2$ is restricted to these two layers (that is, its concentration in layers 3, 4, and 5 is below the limit of detection of 0.05 weight percent). Other major oxides show no consistent trends, with the possible exception of $SO_3$. Microprobe analyses suggest that the bulk $SO_3$ content, which could include both $S^{2-}$ and $SO_4^{2-}$, is slightly higher in the outermost layer, although more analyses are required to fully document its distribution (tables 1, 2). However, S content as $SO_3$ is

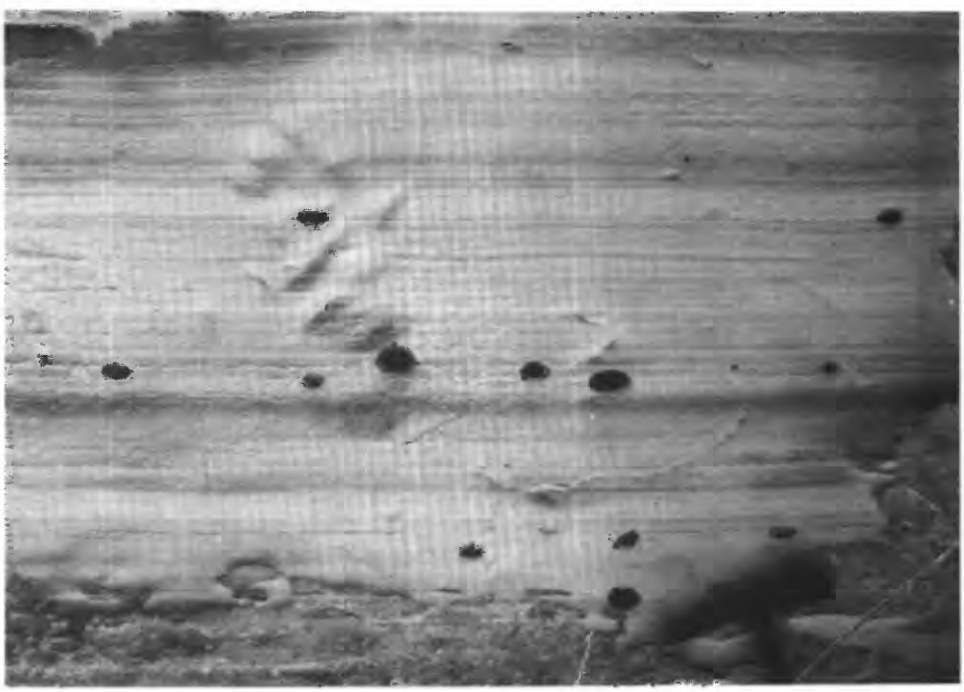

**Figure 2.** Outcrop of Monterey Formation at the Celite mine, showing relation of concretion occurrence to sediment laminations. Hammer at lower right shows scale.

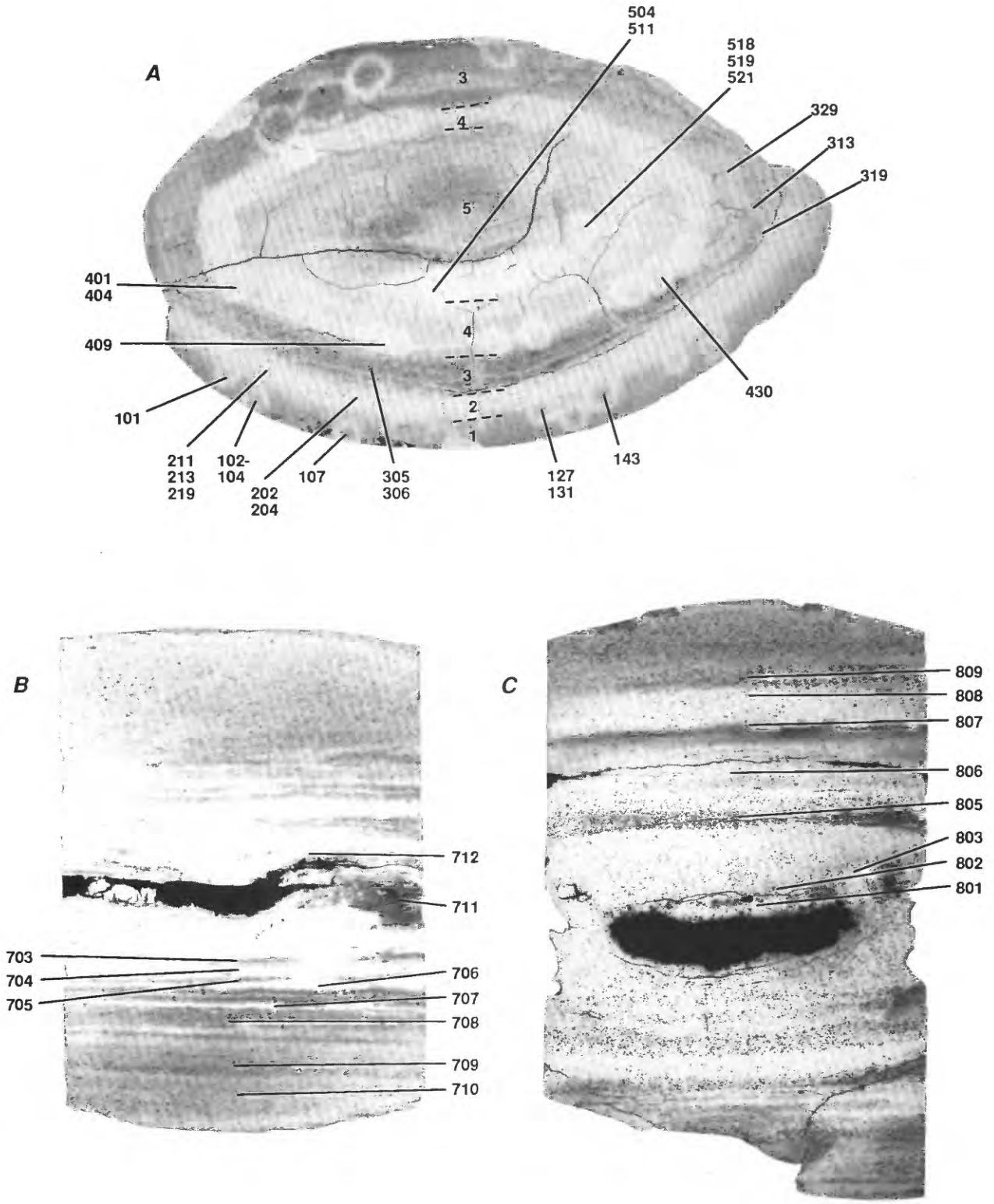


**Figure 3.** Thin-section billets of concretions 5–1 (*A*), 6–A (*B*), and 6–C (*C*) examined by microprobe and SEM-XRF. Three-digit numbers refer to samples listed in table 2. Numbers 1 through 5 in figure 3*A* denote layers referred to in text and in tables 1, 3, 5, and 6; light-colored rings denote areas of microprobe analyses. Alternating light- and dark-colored layers in figures 3*B* and 3*C* reflect alternating dominance of mitridatite and francolite, respectively, and interpretation based on microprobe analyses for Fe and Ca (see table 2) but not on actual XRF analyses. Laminae of dark-colored grains in concretion 6–B represent a high concentration of detrital plagioclase and quartz.

**Table 1.** Bulk composition of individual layers in concretion 5–1

[All values in weight percent; dashes, not analyzed. Major-element oxides determined by XRF analysis, and organic and inorganic $CO_2$ by induction-furnace carbon analyzer. Fe reported as $Fe_2O_3$ except for layer 5. F and $SO_3$ determined by microprobe; values represent averages of all analyses of matrix material, that is, excluding analyses of discrete grains of opal, quartz, and Al silicates. LOI, loss on ignition. Layers refer to concretion shown in figure 3. Clay-shale represents the terrigenous fraction (Isaacs, 1980)]

| Layer----- | 1 | 2 | 3 | 4 | 5 | Clay-shale |
|---|---|---|---|---|---|---|
| $SiO_2$------ | 42.4 | 30.5 | 53.5 | 32.1 | 27.8 | 62.2 |
| $Al_2O_3$----- | 2.5 | 2.0 | 4.6 | 4.5 | 3.7 | 17.8 |
| $Fe_2O_3$----- | 2.8 | 14.9 | 14.1 | 25.4 | -- | 3.6 |
| FeO------- | -- | -- | -- | -- | 26.9 | -- |
| CaO------- | 23.2 | 21.3 | 3.9 | 4.0 | 2.4 | 1.4 |
| MgO------- | .5 | .5 | .7 | .9 | .9 | 2.0 |
| $Na_2O$------ | .5 | .4 | 1.1 | 1.2 | .9 | 2.5 |
| $K_2O$------- | .4 | .3 | 1.6 | 1.6 | 1.5 | 3.6 |
| $P_2O_5$------ | 17.6 | 21.8 | 6.9 | 16.4 | 19.4 | .5 |
| $TiO_2$------ | .1 | .1 | .1 | .1 | .1 | .3 |
| LOI------- | 8.8 | 10.6 | 10.9 | 15.2 | 13.6 | -- |
| $CO_2$ (org)-- | 2.9 | 2.2 | 4.0 | 1.5 | 1.8 | -- |
| $CO_2$ (inorg) | 1.5 | 1.1 | 0 | 0 | 0 | -- |
| F--------- | 1.1 | .6 | .1 | .2 | .1 | -- |
| $SO_3$------- | .5 | .4 | .3 | .2 | .1 | -- |

less than 0.55 weight percent in all microprobe analyses, and no metal sulfides were detected with the SEM, microprobe, or petrographic microscope.

## Minor Elements

The REE contents are similar in all layers except layer 4 (table 3). Shale-normalized REE patterns of layers 1, 2, 3, and 5 show a negative Ce anomaly (a depletion in Ce relative to La and Nd) and an enrichment in heavy REE's (fig. 4) relative to light REE's; this pattern is characteristic of seawater (DeBaar and others, 1985). Normalized REE contents in layer 4 decrease from light to heavy REE's.

Other trace-element contents vary sharply among the layers of concretion 5–1 (table 3). As, Cd, Cu, Zn, and V decrease in content toward the center, whereas Ni and Co show the opposite trend, and Cr content reaches a maximum in layer 3. In all the layers, trace-element contents exceed a possible clay-shale contribution, weighted according to $Al_2O_3$ content (table 1).

## Mineralogy

The mineralogy of each layer in concretion 5–1 (fig. 5) is consistent with variations in the contents of CaO, Fe (both $Fe_2O_3$ and FeO), F, and inorganic $CO_2$, although absolute mineral abundances cannot be inferred from the X-ray diffractograms. Carbonate fluorapatite (McClellan, 1980), commonly referred to as francolite, is the dominant mineral in layer 1. Mitridatite, a calcium-ferric phosphate (Moore, 1980), is the dominant mineral in layer 2, but francolite is also present. Both of these minerals are present in layers 3 and 4, as well as in layer 5. Individual deep-red grains, which are concentrated in an outer 1- to 2-mm-thick band of layer 4, consist of a pure Fe phosphate (their deep-red color indicates that iron is in the 3+ valence

**Table 2.** Partial listing of microprobe analyses of concretions 5–1, 6–A, and 6–B and of phases within the enclosing sedimentary rocks

[All values in weight percent. Locations of samples are shown in figures 3 and 6 except for the 900 series of analyses, which represent the enclosing sedimentary rocks: analyses 900, pelletal phosphate; analyses 910 and 911, dark- and light-colored layers in diatomite, respectively. Asterisks denote analyses used to make calculations listed in table 4]

| Analysis | 101 | 102 | 103 | 104 | 107 | 127* | 131 | 143 | 202 | 204 |
|---|---|---|---|---|---|---|---|---|---|---|
| $SiO_2$--- | 30.2 | 20.1 | 64.5 | 32.1 | 3.56 | 11.7 | 27.2 | 17.8 | 26.2 | 18.5 |
| $Al_2O_3$-- | .45 | 2.83 | 21.9 | .98 | 1.97 | 5.38 | 2.09 | 3.53 | 1.54 | 1.24 |
| FeO---- | 1.20 | 3.33 | .11 | 1.28 | 1.81 | 2.01 | 4.20 | 2.26 | 15.4 | 21.7 |
| MgO---- | .01 | .46 | .01 | .14 | .22 | .75 | .34 | .54 | .28 | .18 |
| $Na_2O$--- | .08 | .28 | 9.32 | .08 | .35 | .33 | .17 | .32 | .19 | .14 |
| $K_2O$---- | .04 | .34 | .12 | .09 | .05 | .90 | .19 | .36 | .20 | .21 |
| CaO---- | 6.36 | 31.8 | 4.71 | 11.2 | 38.7 | 40.3 | 23.9 | 37.5 | 12.6 | 13.4 |
| $P_2O_5$--- | 5.81 | 23.6 | .39 | 8.36 | 30.8 | 29.6 | 19.5 | 27.4 | 17.4 | 22.2 |
| F------ | .36 | 1.93 | .04 | .68 | 2.54 | 2.60 | 1.33 | 2.33 | .46 | .40 |
| $SO_3$---- | .04 | .24 | .04 | .12 | .42 | .14 | .14 | .17 | .09 | .11 |

| Analysis | 211* | 213 | 219 | 305 | 306 | 313 | 319 | 329 | 401 | 404 |
|---|---|---|---|---|---|---|---|---|---|---|
| $SiO_2$--- | 20.1 | 23.0 | 15.7 | 30.1 | 33.8 | 34.5 | 26.6 | 51.5 | 9.36 | 21.4 |
| $Al_2O_3$-- | 1.21 | 2.67 | 2.36 | .83 | 2.31 | 2.72 | 1.12 | 1.64 | 1.08 | 1.37 |
| FeO---- | 23.7 | 19.5 | 13.5 | 9.67 | 9.37 | 19.8 | 16.9 | 12.5 | 43.3 | 34.1 |
| MgO---- | .19 | .40 | .41 | .14 | .38 | .56 | .15 | .17 | .31 | .32 |
| $Na_2O$--- | .17 | .46 | .29 | .16 | .21 | .43 | .08 | .54 | .33 | .41 |
| $K_2O$---- | .29 | .25 | .25 | .10 | .25 | .65 | .12 | .41 | .15 | .18 |
| CaO---- | 12.5 | 15.3 | 26.3 | 3.42 | 3.26 | 7.20 | 3.99 | 4.45 | 4.55 | 3.62 |
| $P_2O_5$--- | 24.0 | 23.0 | 26.2 | 8.87 | 8.00 | 18.0 | 9.55 | 11.2 | 22.4 | 22.8 |
| F------ | .31 | .68 | 1.56 | .12 | .18 | .39 | .19 | .08 | .29 | .29 |
| $SO_3$---- | .05 | .09 | .17 | .19 | .14 | .24 | .09 | .08 | .03 | .05 |

| Analysis | 409* | 430 | 504 | 511 | 518* | 519 | 521 | 703 | 704 | 705 |
|---|---|---|---|---|---|---|---|---|---|---|
| $SiO_2$--- | 4.20 | 1.75 | .98 | 10.7 | 0 | .74 | 0 | 17.6 | 20.4 | 18.5 |
| $Al_2O_3$-- | .50 | 1.85 | .27 | 1.26 | .12 | .11 | .25 | .40 | .40 | 1.30 |
| FeO---- | 43.1 | 32.8 | 46.8 | 36.9 | 42.2 | 37.1 | 42.0 | 2.11 | 23.2 | 1.57 |
| MgO---- | .22 | .39 | .24 | .41 | .12 | .42 | .19 | .37 | .22 | .63 |
| $Na_2O$--- | .40 | .41 | .07 | .13 | .05 | .32 | .09 | .39 | .28 | .44 |
| $K_2O$---- | .19 | .38 | .02 | .19 | .01 | .15 | .01 | .11 | .38 | .31 |
| CaO---- | 4.61 | 12.1 | .28 | .95 | .37 | 9.30 | .26 | 38.1 | 13.0 | 37.2 |
| $P_2O_5$--- | 25.9 | 30.2 | 32.4 | 26.2 | 28.6 | 30.8 | 29.5 | 29.0 | 23.2 | 27.2 |
| F------ | .29 | .72 | .38 | .26 | .30 | .37 | .32 | 3.30 | .51 | 3.02 |
| $SO_3$---- | .01 | .13 | .16 | .09 | .07 | .04 | .13 | .51 | .19 | .64 |

| Analysis | 706 | 707 | 708 | 710 | 711 | 712 | 801 | 802 | 803 | 805 |
|---|---|---|---|---|---|---|---|---|---|---|
| $SiO_2$--- | 17.9 | 20.6 | 18.0 | 16.9 | 6.01 | 19.7 | 7.72 | 2.51 | 5.70 | 26.0 |
| $Al_2O_3$-- | .11 | .29 | .52 | .30 | 1.00 | .60 | .50 | .30 | .30 | .40 |
| FeO---- | 26.5 | 10.5 | 1.33 | .30 | 5.50 | 1.90 | 27.8 | 20.3 | 29.5 | 22.3 |
| MgO---- | .10 | .11 | .44 | .40 | .40 | .30 | .30 | .10 | .40 | .30 |
| $Na_2O$--- | .42 | .09 | .36 | .40 | .40 | .30 | .40 | .10 | .50 | .30 |
| $K_2O$---- | .41 | .08 | .09 | .10 | .40 | .20 | .50 | .10 | .80 | .20 |
| CaO---- | 13.5 | 7.41 | 34.8 | 38.6 | 32.0 | 30.1 | 13.9 | 11.1 | 15.5 | 12.3 |
| $P_2O_5$--- | 25.0 | 12.0 | 26.6 | 26.8 | 25.5 | 21.1 | 24.6 | 19.6 | 28.1 | 23.4 |
| F------ | .41 | .28 | 3.01 | 3.00 | 2.80 | 2.50 | .10 | 0 | 0 | .10 |
| $SO_3$---- | .13 | .11 | .55 | .40 | .30 | .51 | .11 | .01 | .02 | .09 |

| Analysis | 806 | 807 | 808 | 809 | 900* | 910 | 911 |
|---|---|---|---|---|---|---|---|
| $SiO_2$--- | 24.5 | 27.7 | 18.0 | 21.2 | .31 | 52.9 | 45.0 |
| $Al_2O_3$-- | 1.10 | .60 | .80 | 1.30 | .21 | 6.30 | 2.76 |
| FeO---- | 14.7 | 2.60 | 5.60 | 1.80 | .02 | 1.39 | .19 |
| MgO---- | .20 | .10 | .40 | .60 | .10 | .95 | 0 |
| $Na_2O$--- | .20 | .10 | .40 | .50 | .65 | .10 | .03 |
| $K_2O$---- | .20 | .10 | .20 | .30 | .07 | .56 | .04 |
| CaO---- | 8.30 | 1.60 | 35.3 | 37.1 | 51.8 | .50 | .19 |
| $P_2O_5$--- | 14.2 | 2.70 | 27.9 | 27.1 | 36.1 | .15 | .10 |
| F------ | 0 | 0 | 1.70 | 1.90 | 3.73 | .07 | .02 |
| $SO_3$---- | .02 | .01 | .52 | .38 | 1.91 | .13 | .06 |

**Table 3.** Trace-element composition of concretion 5–1

[All values in parts per million. Dashes, not analyzed; n.d., no data available. Trace-element analyses (duplicates in parentheses) by inductively coupled plasma optical-emission spectroscopy (ICP–OES); limits of detection: As, 1; Cd, 2; Ce, 4; Co, 1; Cu, 1; La, 20; Nd, 20; Ni, 2; V, 2; Yb, 1; Zn, 4 Lichte and others, 1987; Taggert and others, 1987). Rare-earth-element analyses (in brackets) by ICP–OES after group separation; limits of detection: Ce, 0.15, Er, 0.04; Eu, 0.004; Gd, 0.09; Ho, 0.02; La, 0.02; Lu, 0.009; Nd, 0.01; Pr, 0.3; Sm, 0.15; Yb, 0.01 (Crock and Lichte, 1982). Layers refer to concretion shown in figure 3. Analyses of clay-shale from Haskin and Haskin (1966) and Wedepohl (1969); analyses of organic matter from Elderfield and others (1981) and Brumsack (1986)]

| Layer-- | 1 | 2 | 3 | 4 | 5 | Clay-shale | Organic matter |
|---|---|---|---|---|---|---|---|
| La----- | -- | [17] | [15] | [28] | [7.7] | 41 | 0.014 |
| | (27) | (23) | -- | -- | -- | | |
| Ce----- | -- | [24] | [20] | [38] | [11] | 83 | n.d. |
| | (35) | (27) | -- | -- | -- | | |
| Pr----- | -- | [3.6] | [2.1] | [3.3] | [1.4] | 10.2 | n.d. |
| Nd----- | -- | [18] | [11] | [8.1] | [4.8] | 38 | n.d. |
| | (30) | (22) | -- | -- | -- | | |
| Sm----- | -- | [3.5] | [2.1] | [0.8] | [0.7] | 7.5 | n.d. |
| Eu----- | -- | [0.9] | [0.6] | [0.2] | [0.2] | 1.61 | n.d. |
| Gd----- | -- | [5.8] | [5.4] | [0.5] | [1.4] | 6.5 | n.d. |
| Ho----- | -- | [1.2] | [0.58] | -- | [0.37] | 1.34 | n.d. |
| Er----- | -- | [4.8] | [2.7] | [0.2] | [1.5] | 3.75 | n.d. |
| Yb----- | -- | [5.2] | [3.0] | [0.24] | [1.2] | 3.53 | n.d. |
| | (7) | (7) | -- | -- | -- | | |
| Lu----- | -- | [1.0] | [0.6] | -- | [0.2] | .61 | n.d. |
| As----- | -- | 2,000 | 1,500 | 640 | 580 | 10 | 6 |
| | (80) | (450) | -- | -- | -- | | |
| Cd----- | -- | 1,500 | 700 | 300 | 70 | .3 | 12 |
| | (650) | (950) | -- | -- | -- | | |
| Co----- | 7 | 17 | 11 | 21 | 51 | 19 | 1 |
| | (6) | (14) | -- | -- | -- | | |
| Cr----- | 55 | 150 | 520 | 96 | 17 | 83 | 2 |
| | (56) | (89) | -- | -- | -- | | |
| Cu----- | 36 | 46 | 37 | 20 | 12 | 35 | 11 |
| | (51) | (50) | -- | -- | -- | | |
| Ni----- | 76 | 180 | 210 | 330 | 720 | 42 | 7 |
| | (150) | (170) | -- | -- | -- | | |
| V------ | 220 | 290 | 220 | 150 | 89 | 110 | 3 |
| | (320) | (340) | -- | -- | -- | | |
| Zn----- | 1,250 | 2,000 | 470 | 700 | 500 | 100 | 110 |
| | (1,200) | (1,400) | -- | -- | -- | | |

state) that proved to be amorphous when X-rayed separately (R. Erd, oral commun., 1991); this phase is referred to below as amorphous ferric phosphate (AFP). Vivianite, a ferrous phosphate, is the dominant mineral in layer 5.

## MINERAL STOICHIOMETRY

The stoichiometry of each phosphate phase (table 4) was calculated from microprobe analyses of concretion 5–1 (table 2) by using a normative scheme. Individual analyses selected for making the calculations represent the most phosphate enriched analyses with the largest sum of total oxides. In layers 1 and 2, we could not locate individual grains of pure francolite and mitridatite, possibly owing to their smallness and the pervasiveness of fine-grained, detrital Al-silicate minerals and diatomaceous material. In layers 4 and 5, the analyses used were of what appeared under the microprobe and SEM (fig. 6) to be individual mineral grains.

Our calculations are based on several assumptions. (1) All $Al_2O_3$ is present in a terrigenous Al-silicate fraction,

**Table 4.** Stoichiometry of major phosphate phases in concretion 5–1, of a pelletal phosphate grain with diatomite, and of a metal oxide in concretion 6–B

[See table 2 (asterisks) for microprobe analyses. $CO_2$ contents in concretionary francolite from table 1. $CO_2$ was added to achieve charge balance for pelletal phosphate, $H_2O$ was determined by forcing sums to 100 percent, and $OH^-$ was added to achieve charge balance]

| | |
|---|---|
| Concretionary francolite: | |
| This study | $Ca_{10.1}(PO_4)_{5.8}(CO_3)_{0.4}F_{2.0}$ |
| Mitridatite: | |
| This study | $^1Ca_4(H_2O)_6Fe_{10.6}O_6(PO_4)_{9.3}\cdot 7H_2O$ |
| Moore (1980) | $Ca_6(H_2O)_6Fe_9O_6(PO_4)_9\cdot 3H_2O$ |
| Amorphous ferric phosphate (oxykertschenite): | |
| This study | $Fe_3(OH)_{4.2}(PO_4)_{1.6}\cdot 5.5H_2O$ |
| Moore (1980) | $Fe_3(OH)_3(PO_4)_2\cdot 5H_2O$ |
| Vivianite: | |
| This study | $Fe_3(PO_4)_2\cdot 7.8H_2O$ |
| Dana (1935) | $Fe_3(PO_4)_2\cdot 8H_2O$ |
| Metal oxide: | |
| This study | $^2Mn_{10}Ni_5ZnO_{26-x}$ |
| Pelletal francolite: | |
| This study | $Ca_{9.1}Na_{2.2}(PO_4)_{5.5}(SO_4)_{0.3}(CO_3)_{0.6}F_{2.1}$ |
| McClellan (1980) | $Ca_{10-x-y}Na_xMg_y(PO_4)_{6-z}(CO_3)_zF_{2+0.4z}$ |

[1]Additional analyses suggest that mitridatite contains as much as 30 mol $H_2O$.

[2]The value of $x$ corrects the stoichiometry of this phase for the valence of Mn, which, on the basis of laboratory studies, is likely between 3+ and 4+ (Hem and others, 1987, 1989).

with the same major-element-oxide proportions as those of clay-shale (table 1; Isaacs, 1980). Discrepancies in the oxide:$Al_2O_3$ ratios with clay-shale reflect variations in the composition of the clay-shale fraction and analytical errors at low $K_2O$, $Na_2O$, and MgO contents. Short-range variation in composition is clearly represented by discrete laminae composed largely of fine-grained quartz and plagioclase (fig. 3). The bulk of the terrigenous fraction, however, is considered to have a composition close to that of ideal clay-

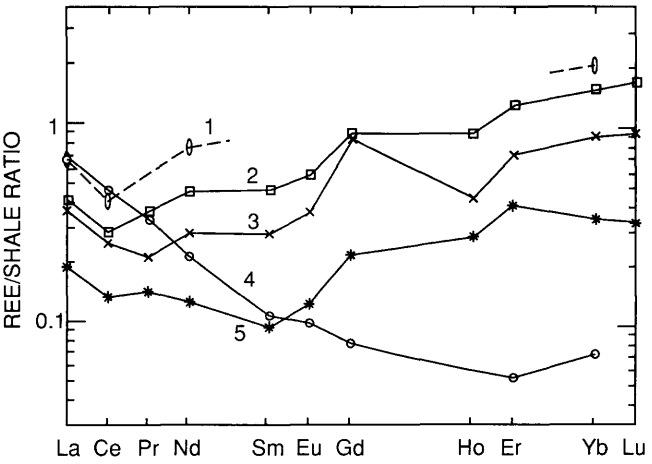


**Figure 4.** REE patterns in concretion 5–1. Numbers refer to layers 1 through 5 in figure 3*A*. Analyses normalized to shale values on an element-by-element basis (see table 3).

**Table 5.** Partial listing of semiquantitative SEM-XRF analyses of concretions 5–1, 6–A, and 6–B

[All values except for SI ($SiO_2$:$Al_2O_3$ ratio) in atomic percent; dashes, not detected. $Na_2O$, $K_2O$, and MgO were not detected in any analyses; the limit of detection for these major-element oxides was approximately 0.7 weight percent, as determined by analysis of pure Al-silicate phases. See figure 6 for locations of samples]

| Analysis- | A-1 | B-1 | B-2 | B-3 | C-1 | D-1 | D-2 | E-1 | E-2 | E-3 | F-1 |
|---|---|---|---|---|---|---|---|---|---|---|---|
| Al------- | 1.41 | .59 | 1.30 | 2.83 | -- | -- | 1.18 | 0.84 | 3.91 | 2.64 | 4.74 |
| Si------- | 4.26 | 2.13 | 3.83 | 8.45 | 8.20 | .62 | 2.35 | 2.42 | 3.87 | 4.01 | -- |
| P-------- | 32.4 | 36.1 | 34.4 | 32.4 | 38.2 | 38.4 | 39.7 | 37.9 | 38.9 | 36.2 | -- |
| Ca------- | 55.3 | 20.9 | 20.3 | 39.9 | 21.4 | 4.60 | -- | -- | -- | 12.0 | 2.43 |
| Mn------- | -- | -- | -- | -- | -- | -- | -- | -- | -- | -- | 52.2 |
| Fe------- | .8 | 35.3 | 32.8 | 12.1 | 32.2 | 59.4 | 45.9 | 46.0 | 45.2 | 34.6 | 3.3 |
| Zn------- | -- | -- | -- | -- | -- | -- | -- | -- | -- | -- | 4.8 |
| Ni------- | -- | -- | -- | -- | -- | -- | -- | -- | -- | -- | 22.1 |
| SI------- | 3.5 | 4.2 | 2.2 | 3.5 | -- | -- | 2.3 | 3.3 | 1.2 | 1.8 | -- |

shale. In support of this interpretation, the range in $SiO_2$:$Al_2O_3$ weight ratios of material filling diatom frustules (fig. 6; table 5) is within the range of the estimated ratios for terrigenous clay-shale of 3.5:1 and its Al-silicate fraction of 2.1:1; the difference between these two values represents the amount of detrital quartz present in clay-shale. (2) The $SiO_2$ in excess of the 3.5:1 ratio corresponds to the amount of biogenic opal-A (that is, diatomaceous material) present (Isaacs, 1980). (3) All of the F is in francolite. (4) The Fe in excess of an $Fe_2O_3$:$Al_2O_3$ ratio of 0.202, the clay-shale contribution (table 1), is in a phosphate phase. Finally, (5) water was added to bring all totals to 100 weight percent; the amount present as $OH^-$ was assessed to balance charge in the phosphate phases, except for francolite.

## Francolite

The stoichiometry of francolite was determined from analysis 127 of layer 1 (table 2). Iron in this analysis can be partitioned into the Al silicates with a residual $Fe_2O_3$ content of only 0.8 weight percent. Charge balance in francolite was achieved by including inorganic $CO_2$, as

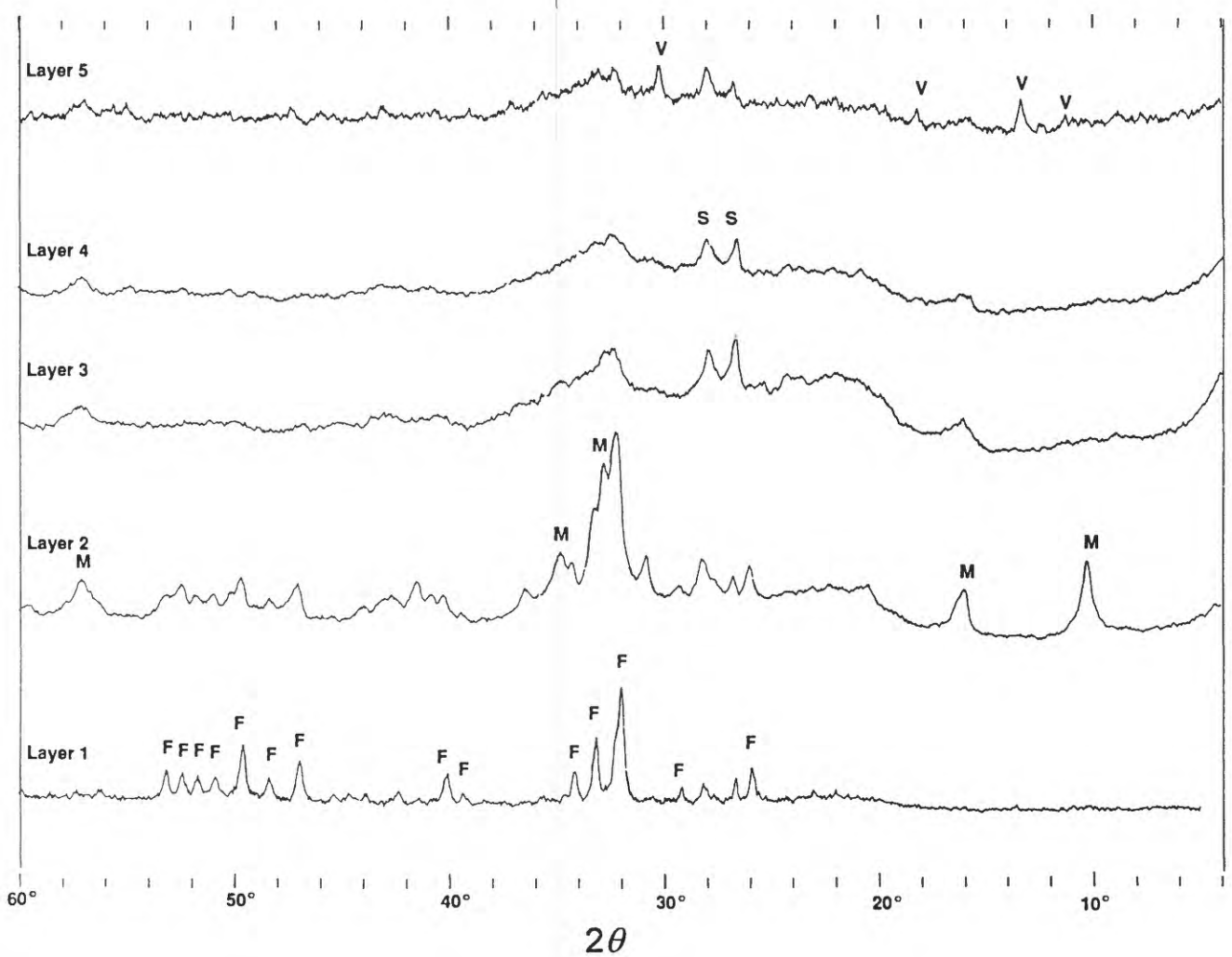


**Figure 5.** XRD patterns in concretion 5–1. Numbered layers are shown in figure 3*A*. F, francolite; M, mitridatite; S, feldspar; V, vivianite.

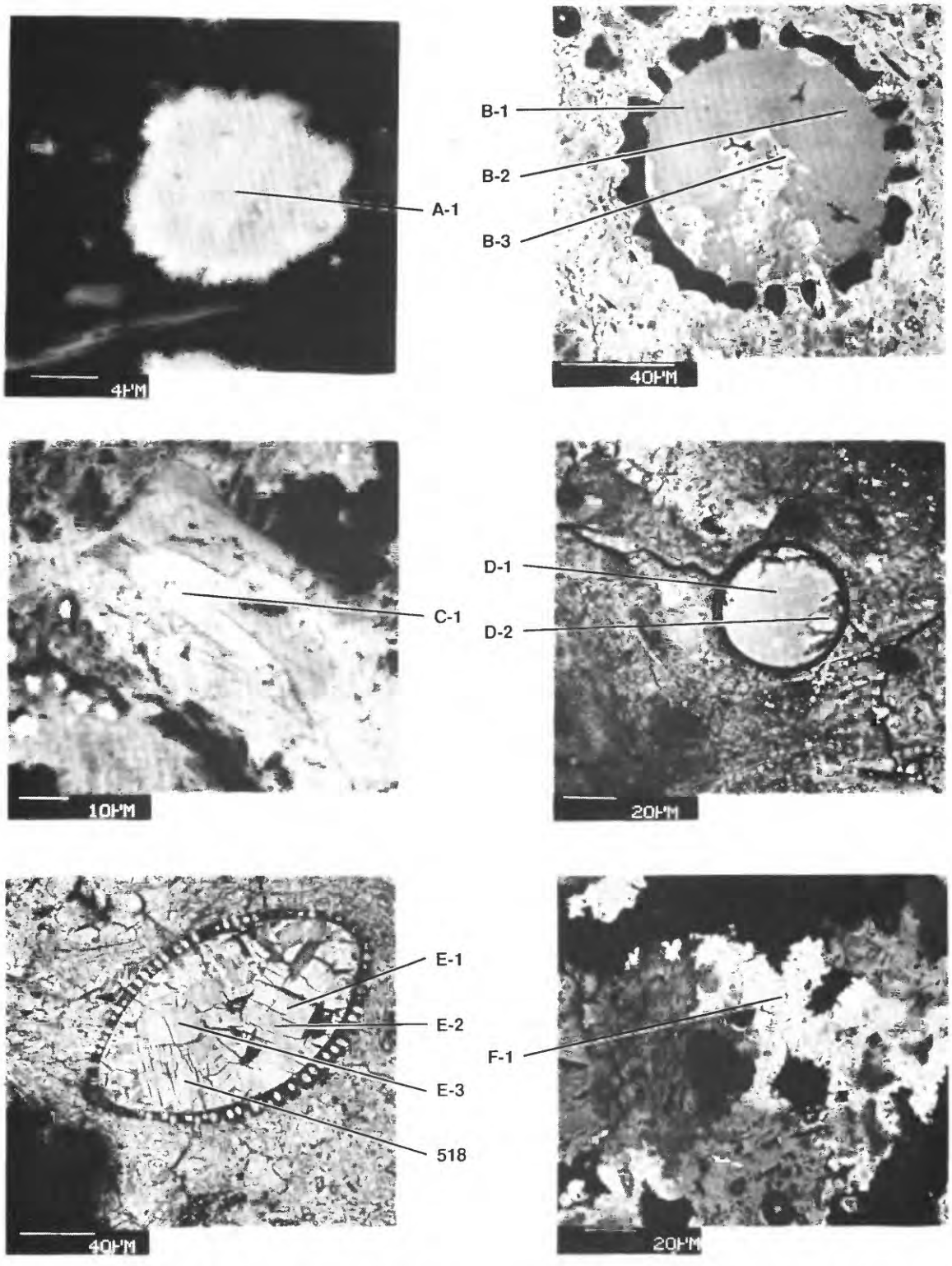


**Figure 6.** Backscatter SEM photographs of concretions within the Monterey Formation, showing locations of samples analyzed in tables 2 and 5. *A*, Francolite in layer 1 of concretion 5–1. *B*, Francolite (light-colored areas) and mitridatite (dark-colored areas) in a radiolarian (black areas) filling in concretion 6–B. An intimate association of these two minerals is visible along lower outer edge of radiolarian. *C*, Mitridatite lath in a diatom test, with porous background. *D*, AFP (light-colored area in a diatom filling) associated with CaO-depleted mitridatite(?) in layer 4 of concretion 5–1. *E*, Vivianite (light-colored area) associated with mitridatite (dark-colored area) in a radiolarian filling in layer 5 of concretion 5–1. *F*, $Mn_{10}Ni_5ZnO_{26-x}$ lining a cavity in concretion 6–A.

$CO_3^{2-}$, in the amount measured in layer 1 (table 1). Inorganic $CO_2$ was partitioned into this mineral (table 4), owing to its absence in the bulk analyses of layers 3, 4, and 5 (table 1) and our failure to detect any carbonate minerals within the concretion. A difference in spacing of the 004 and 410 XRD reflections of 1.5° 2θ further supports the inclusion in francolite of approximately 1.5 weight percent $CO_2$ as $CO_3^{2-}$ (Gulbrandsen, 1970; Schuffert and others, 1990).

SEM-XRF analyses of a relatively pure mineral grain (fig. 6*A*; table 5) confirmed the Ca:P atomic ratio of this calculation. Also, no Mg, K, or Na was detected by SEM-XRF in excess of the Al-silicate contribution. This stoichiometry agrees closely with the published values for pelletal marine francolite (table 4), except for the absence of $Na^+$, $Mg^{2+}$, and $SO_4^{2-}$ substitutions (McClellan, 1980; Nathan and Neilsen, 1980).

## Mitridatite

The stoichiometry of mitridatite was determined from analysis 211 (table 2) by assuming that it and francolite are the only mineral phosphates in layer 2 (fig. 5). SEM–XRF analysis of a single mineral grain (fig. 6) gave an Fe:Ca:P ratio of 10:6.7:12 (table 5), which approximates the literature value (table 4). Microprobe and SEM–XRF analyses of other grains indicate, however, that this Fe:Ca ratio represents a minimum.

The backscatter SEM image shows an intimate association of francolite and mitridatite in concretion 5–1 and the other concretions as well. This association is best shown in figure 6*B*, along the outer part of the diatom test, where francolite is the brighter phase. Its higher reflectivity requires that it has a higher mean atomic number than mitridatite, but the microprobe analysis (tables 2, 4) requires the opposite. One possible way to lower the mitridatite mean atomic number is to add water. Other microprobe analyses of concretions 5–1, 6–A, and 6–B suggest that mitridatite's formula contains as many as 30 mol $H_2O$, or $Ca_4(H_2O)_6Fe_{10.3}O_6(PO_4)_9{\cdot}30H_2O$. Although its mean atomic number is less than that of francolite, its $H_2O$ content, which is very weakly constrained by the method we have used to estimate it in this and other phases, greatly exceeds that reported by Moore (1980).

## AFP and Vivianite

The stoichiometry of AFP (analysis 409, table 2) approaches that of oxykertschenite, an amorphous phase formed through the oxidation of vivianite (Moore, 1980). Vivianite, despite its blue color, has the classical composition of $8H_2O$, with no $OH^-$ ions needed to balance charge, in contrast to the stoichiometry favored by Tien and Waugh (1969) for a blue vivianite.

**Table 6.** Major mineral fractions of individual layers in concretion 5–1

[All values in weight percent, rounded to the nearest 5 weight percent. See table 1 for major-element-oxide analyses]

| Layer---------- | 1 | 2 | 3 | 4 | 5 |
|---|---|---|---|---|---|
| Francolite------ | 35 | 25 | 5 | 5 | 5 |
| Mitridatite----- | 5 | 35 | 20 | 5 | 0 |
| AFP------------- | 0 | 0 | 10 | 50 | 0 |
| Vivianite------- | 0 | 0 | 0 | 0 | 60 |
| Biogenic silica- | 35 | 25 | 40 | 15 | 15 |
| Clay-shale------ | 15 | 15 | 25 | 25 | 20 |
| Calcite--------- | 0 | 0 | 0 | 0 | 0 |

Semiquantitative SEM–XRF analyses of vivianite (table 5) suggest that some $Fe^{3+}$ may be present, which would be balanced by the addition of $OH^-$. The Fe:P atomic ratio is 9:8, somewhat larger than that of 9:6 from microprobe analyses. In both data sets, the ratio is the same in the two phases.

## Mn-Ni-Zn Oxide

The only metal oxide or sulfide detected (fig. 6*F*; analysis F–1, table 5) is an Mn-Ni-Zn oxide, which occurs as the lining of a cavity within concretion 6-A and has an Mn:Ni:Zn atomic ratio of approximately 10:5:1. Its high electron backscatter precludes its presence as a carbonate. Charge balance was achieved with 26 oxygen atoms (table 4), by assuming that Mn is in the 4+ valence state, although it is much more likely to have an average valence between 3+ and 4+ (Hem and others, 1987, 1989).

## Mineral Distributions

The average abundances of minerals and clay-shale in the layers of concretion 5–1 were determined from bulk analyses (table 1) by assuming a constant stoichiometry for each phase (table 4). These calculated mineral distributions (table 6) are supported by X-ray diffractograms (fig. 5). We note a change of the dominant phosphate phase, from vivianite in layer 5 to francolite in layer 1, as well as minor amounts of francolite and mitridatite in layers 3, 4, and 5. Also, the clay-shale:biogenic-silica ratio, based on major-element-oxide analyses, is significantly smaller in the outer than in the inner two layers.

Microprobe analyses of concretions 6–A and 6–B (fig. 3; table 2), in which only francolite and mitridatite were detected by XRD, show a different distribution. The two minerals alternate in dominance between successive layers, but the abundance of francolite still increases in the outermost layers, on the basis of an outward overall increase in Ca:Fe ratio and F content (700 and 800 series of analyses, table 2).

## PELLETAL PHOSPHATE GRAINS

Grains of pelletal phosphate also were observed in thin sections of the diatomite. The pellets are 1 mm in diameter and constitute less than 1 volume percent of the total sedimentary rock. The absence of Fe, a high F content, and an F:P atomic ratio of 0.26 (analysis 900, table 2) all require that francolite is the only phosphate mineral present. Its composition, however, corrected for a minor contribution of oxides from Al silicates, differs from that of francolite within the concretions (table 4): The pelletal francolite has $Na^+$ and $SO_4^{2-}$ contents typical of marine francolite (McClellan, 1980; Nathan and Neilsen, 1980).

## DISCUSSION

The host sediment of the concretions consists mainly of diatomite, diatomaceous shale, and diatomaceous mudstone (Isaacs, 1989) that contain traces of pelletal phosphate. The abundance of terrigenous debris ranges from as little as 10 weight percent in some mined crudes to 50 weight percent or more in other beds. Strata are thinly laminated (fig. 2) in the area from which the concretions were recovered. Darker colored laminae contain slightly more terrigenous material and organic matter than lighter colored laminae (Donegan and Schrader, 1981). Donegan and Schrader favored accumulation on an open shelf, impinged by an intense $O_2$-minimum layer, similar to conditions in the Gulf of California (Calvert, 1964). Govean and Garrison (1981) and Pisciotto and Garrison (1981) favored a poorly aerated, deep-water marine basin, as proposed initially by Bramlette (1946).

The laminar structure of the diatomite is unaffected by the presence of the concretions we have examined (fig. 2). Laminae exhibit no compaction features about the concretions and pass through several concretions with no change in thickness. Because the porosities of diatomaceous sediment are unusually high (Hamilton, 1976; Isaacs, 1981), laminae in the diatomite would show distinct draping around concretions that formed in uncompacted sediment, with thicknesses as little as a fourth to a third those of laminae possibly preserved within the concretions. Thus, these concretions must have formed after the sediment was fully compacted.

The concretions could have formed near maximum depth of burial within the marine environment, where an absence of bedded opal-CT strata restricts depth of burial to less than approximately 800 m for a geothermal gradient of 50 to 67°C/km (Keller and Isaacs, 1985). Conversely, they could have formed during uplift into their present terrestrial setting, beginning 4–2 Ma (Namson and Davis, 1990). Thus, their mineralogy and minor-element composition might represent a part-freshwater, part-seawater origin. Alternatively, the concretions could have formed totally within a freshwater environment, despite the strong marine signal. In either case, their mineralogy and elemental composition are unrelated, at least directly, to the environment of sediment deposition.

### Mineral Paragenesis

On the basis of mineral distributions within the concretions (table 6), paragenesis of the phosphatic and metal-oxide phases is represented by the following scheme:

vivianite - AFP - mitridatite - francolite - $Mn_{10}Ni_5ZnO_{26-x}$,

where $x$ corrects for an average valence of less than 4+ for Mn. The natural occurrences and thermodynamic properties of these minerals require that this sequence represents a change in pore-water chemistry from reducing and virtually neutral pH to oxidizing and alkaline. Vivianite, which constitutes the nucleus of concretion 5–1, was the initial precipitate; it has been reported in lake and estuarine sediment and in soils (Rosenqvist, 1970; Nriagu, 1972; Hearn and others, 1983; Henderson and others, 1984). On the basis of these occurrences, vivianite precipitates under the most reducing conditions and at the lowest pH of all the minerals observed. The absence of Al-phosphate phases probably limits the pH (Altschuler, 1973) to no less than about 6.5.

AFP might represent a separate phase or, alternatively, an oxidation product of vivianite. The similar Fe:P ratio for these two phases (table 4) and the similarity of their blocky morphology (compare the habit of AFP in fig. 6*D* along the top and right edges of the diatom filling with that of vivianite in fig. 6*E*) argues strongly for the interpretation of AFP as an oxidation product, whereas the strong difference in REE patterns of the two phases (fig. 4)—that is, REE fractionation between different solid phases—favors its interpretation as a separate phase. If AFP represents a separate phase, then its precipitation might have required a change in pore-water pH but, more clearly, would have required an increase in Eh.

Both increasing Eh and increasing pH, as well as freshwater conditions, are required for the precipitation of mitridatite (Nriagu and Dell, 1974; Moore, 1980). The freshwater conditions for all three Fe-phosphate phases could have been achieved by uplift into the terrestrial ground-water environment beginning 4–2 Ma (Namson and Davis, 1990).

The dominance of francolite in the outer layers of all concretions requires that it was the final phosphate to precipitate. Its dominance would have required a continuation in the trend of increasing pH but not necessarily Eh. Within modern sediment on the Peru shelf, francolite precipitates within the uppermost few centimeters of the sea floor (Froelich and others, 1988)—within the suboxic zone of

denitrification (McArthur and others, 1986)—and, possibly, under oxic conditions on the sea floor. In major marine phosphorites, in which francolite is the dominant phosphate phase (McClellan, 1980), the $\delta^{34}S\text{-}SO_4^{2-}$ value of francolite requires formation throughout the Eh range from oxygen respiration to sulfate reduction (Piper and Kolodny, 1988). If these depositional environments define the chemistry of francolite precipitation in the concretions within the Monterey Formation, then the pore water must have had a pH higher than approximately 7.6—that is, strongly alkaline—but an Eh that could have varied over the entire range of Fe-phosphate stabilities. They also would seem to require marine conditions.

Seawater intrusion into fresh-ground-water systems of southern California is a well-documented phenomenon (Los Angeles County Flood Control District, 1957). Such intrusion into the Monterey Formation during uplift might account for the distribution of francolite in these concretions.

The difference between the compositions of concretionary francolite and of pelletal francolite dispersed in the diatomite suggests that an origin requiring introduction of seawater may not be the simplest explanation. The pelletal francolite has high $Na^+$ and $SO_4^{2-}$ contents (tables 2, 4), similar to those in francolite of major marine deposits. Both ions are highly concentrated in seawater. Thus, the absence of these ions in the concretionary francolite indicates that it precipitated within the same freshwater environment in which vivianite and mitridatite precipitated.

The trace amount of $Mn_{10}Ni_5ZnO_{26-x}$ in concretion 6–A (fig. 6*F*) required an increase in both Eh and pH for its precipitation. Hem and others (1987, 1989) precipitated several Mn oxides in the laboratory. Under fully oxidizing, freshwater conditions and at a pH of approximately 7.8 and higher, the average Mn valence is between 3+ and 4+. Although these experiments support an interpretation of continuously increasing Eh and pH, they probably are only weakly analogous to natural systems. For example, the high Ni content in this precipitate greatly exceeds that in laboratory studies, which tend to show very limited substitution in the β-MnOOH lattice from a solution with an Ni concentration sufficient to precipitate $NiO_2$ (Hem and others, 1989).

Paragenesis of the concretions can be depicted on a stability diagram (fig. 7), adapted from Nriagu and Dell (1974), for which Eh and pH are variables. Other topologic projections plot different variables (Viellard and others, 1979). All of these projections, however, are limited by the requirement in their construction to hold constant activities of various aqueous components.

The broad stability field of francolite, albeit based on its occurrence in the marine environment, and the absence of Fe oxides in association with Mn oxide suggest that $Ca^{2+}$, $Fe^{2+}$, $F^-$, and $Mn^{2+}$ contents, as well as Eh and pH, changed continuously. For example, francolite occurs with pyrite in Peru shelf sediment (Piper and others, 1988) at the one extreme of Eh, and with ferromanganese deposits (Manheim and others, 1980) at the other extreme. Using Nriagu and Dell's (1974) values for $Ca^{2+}$ and $PO_4^{3-}$ activities and an F:Ca ratio of 0.01 in solution (as estimated from the mass ratio of biogenic calcite), the ion-activity product should have exceeded the solubility product of francolite (Jahnke, 1984). Thus, francolite should have precipitated throughout the Eh-pH field of stability of Fe phosphates, and it should be abundant in all layers, not merely in the outermost layer. Its minor occurrence in the interior of concretion 5–1 (table 6) probably represents precipitation at the time of accretion of layer 1, by merely an infilling of residual porosity, rather than coprecipitation with vivianite, although we cannot rule out this possibility. Its precipitation in the absence of Fe oxides, unequivocally after mitridatite in all concretions, is most easily explainable by a decrease in $Fe^{2+}$ activity and an increase in $Ca^{2+}$ and $F^-$ activities.

Despite the stability diagram's (fig. 7) limitations to a natural system, it nonetheless identifies the changes in Eh and pH required to precipitate vivianite initially and an Mn oxide ultimately. Failure to detect the other phosphate minerals reported by Nriagu and Dell (1974), such as lipscombite and foucherite, may be due to the poor detection limit of XRD, or the substitution of lipscombite by AFP.

## Elemental Sources

REE patterns further define the conditions under which the concretions formed. The REE patterns of vivianite,

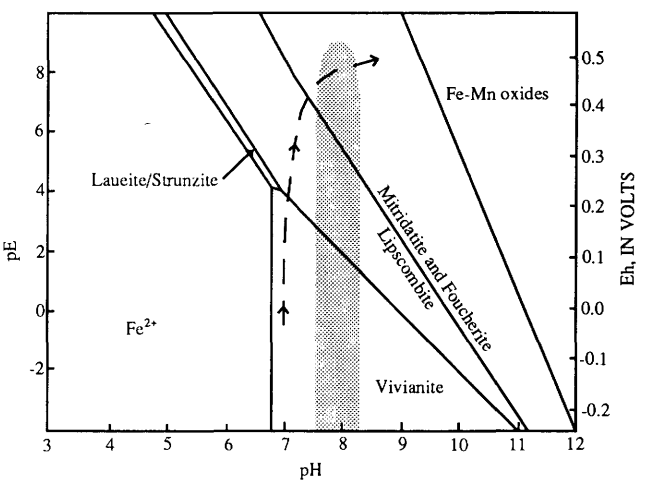


**Figure 7.** Stability relations between Fe-Mn oxides and phosphate minerals at $PO_4^{3-}$, $Fe^{2+}$, $Ca^{2+}$, and $Mn^{2+}$ activities of $10^{-6}$, $10^{-4}$, $10^{-3}$, and $10^{-4}$, respectively (adapted from Nriagu and Dell, 1974). Shaded area, approximate field of occurrence of francolite in modern marine environment; dashed line, possible trend of pore-water chemistry during formation of concretion 5–1 (fig. 3).

mitridatite, and francolite (fig. 4) strongly resemble that of seawater (De Baar and others, 1985) and marine biogenic phases—$CaCO_3$ (Palmer, 1985), opal, and, possibly, organic matter (Elderfield and others, 1981)—showing a strong negative Ce anomaly and an enrichment of heavy over light REE's. Because Fe phosphates have been reported only in freshwater deposits, to our knowledge, the original source of the REE's could not have been seawater. Concretion formation late in the diagenetic history of the diatomite would have allowed for the immediate REE sources to have included pyrite, various alteration products of organic matter (Odermatt, 1986), and adsorbed phases. The most likely original source for REE's, however, was remobilized biogenic phases. For example, marine siliceous ooze, consisting of opal-A, can have an La content as great as 5.8 ppm (Elderfield and others, 1981). Opal-A is the dominant phase in these rocks, which show abundant evidence of its dissolution (fig. 6). Organic matter, with an La content of only 0.14 ppm (Elderfield and others, 1981), and $CaCO_3$, with an La content of 0.13 ppm (Palmer, 1985), would have supplied only a minor fraction.

The source of other minor elements also was likely biogenic phases. Within the open ocean today, the Ni and Zn contents of seawater increase with depth. Their distributions closely parallel the seawater profile for silica (Sclater and others, 1976), suggesting that their pathway in seawater is coupled to that of biogenic silica. The distributions of Cd, Cr, Cu, and V in seawater resemble those of $NO_3^-$ and $PO_4^{3-}$, the two essential nutrients for biologic productivity.

The relative concentrations of trace elements are unusual. Within marine organic matter, the content of Cu is approximately the same as that of Cd and significantly greater than those of other minor elements (table 3) except Zn (Martin and Knauer, 1973; Collier and Edmond, 1984; Brumsack, 1986). The average content of Cu in concretion 5–1, however, is much smaller than those of other minor elements. The phases in which minor elements occur, as well as their sources, clearly must be ascertained to fully understand their incorporation into the concretions. We propose that both REE's and Ni had a largely biogenic silica source, and so they might have been expected to show similar trends in concretion 5–1; yet they show opposite trends (table 3) if the REE contents of layer 4 are discounted. REE and Ni contents must be influenced by their source, although the distribution of REE's may be dominated by their substitution for $Ca^{2+}$ in francolite (Altschuler and others, 1967).

The source of major constituents also was probably the biogenic phases. The average P content of marine organic matter is 0.76 weight percent (Brumsack, 1986). Although the organic-matter content of the Monterey Formation is as great as 25 weight percent, it averages only about 3 weight percent in unweathered strata at the diatomite quarry (C.M. Isaacs, unpub. data, 1991). Even at this lower concentration, marine organic matter within the sedimentary rocks would have been an adequate source for P in the dispersed concretions of this formation. These concretions have been reported only in this section of the Monterey Formation, and they are widely spaced (fig. 2). A possible alternative immediate source for P was an adsorbed phase on clay minerals (Schultz and others, 1980), but the original source still was likely organic matter.

The source of Fe could have been either organic matter or pyrite, which has been widely reported in the Monterey Formation and can decompose before the complete oxidation of organic matter (Littke and others, 1991). The Fe content of marine organic matter ranges from approximately 50 to 3,000 ppm (Martin and Knauer, 1973) but commonly is less than 500 ppm. Thus, the Fe:P weight ratio in organic matter (approx 0.1) is less than in vivianite (approx 5). If the major source of both Fe and P was organic matter, rather than pyrite and an adsorbed component on clays, then this difference in the weight ratios suggests that initial formation of the concretions—that is, the precipitation of vivianite and AFP—was Fe limited rather than P limited. Although the probable availability of Fe and P from other phases weakens this argument, the absence of Fe-oxide and Fe-sulfide phases seems to support it.

Dissolution of $CaCO_3$ during continued uplift into the freshwater environment could have been the source of increasing pH, as well as of $Ca^{2+}$. In the diatomite, the $CaCO_3$ content is less than about 0.1 weight percent, whereas $CaCO_3$ is a major component in subjacent strata of the Monterey Formation (Isaacs, 1980, 1989; Govean and Garrison, 1981; Pisciotto and Garrison, 1981).

Dissolution of $CaCO_3$ also could have provided $F^-$. The average F content in carbonate tests of marine plankton is approximately 0.1 weight percent (Carpenter, 1969). Piper and others (1990) showed that $CaCO_3$ dissolution easily provided the $F^-$ for precipitation of francolite in the insular phosphate deposit on Nauru, also under freshwater conditions. The $F^-$:$Ca^{2+}$ ratio in carbonates, however, is much lower than in concretionary francolite (0.002 versus 0.2, respectively). Thus, precipitation of francolite may have been limited by the availability of $F^-$.

## Mass Transport

We have addressed above the chemical properties of the environment and the source of ions. We might ask why the concretions within the Monterey Formation formed at all and why they formed where they did, instead of the ions merely diffusing through the system and then being lost at the surface to streams, as must be the rule rather than the exception. Clearly, diffusion through the diatomite was interrupted and precipitation enhanced by some

chemical boundary, or chemical gradient. This condition must prevail for all concretionary deposits, whether they formed on the sea floor, within the sediment after burial, within the sedimentary rock after compaction, or at the Earth's surface after uplift and erosion. Such a boundary is more easily visualized in the first and last cases, but they are present throughout sediment and sedimentary-rock sections as well.

The chemical gradient—that is, mass transport—is the essential ingredient for concretionary growth; it could have been one of Eh, pH, alkalinity, or concentrations of other ions. Both ground-water recharge and tectonic uplift could have acted to shift up or down such gradients. The size of the concretions and the thickness of individual layers, however, must somehow reflect the stability of the system. Without any knowledge of the rate of concretionary growth, of tectonic uplift, or of ground-water recharge at the time of accretion, we can only speculate in general terms about conditions at the sites of accretion. The distribution of minerals alone, however, suggests that the site of formation of such concretions as 5–1 (fig. 3) differed from that of concretions 6–A and 6–B. The environment of accretion for concretion 5–1 moved in a single direction, in steps, with intervening periods of stability. The flux of ions might have been dominated by diffusion, which was interrupted by tectonics—that is, uplift. In contrast, the environment of accretion for such concretions as 6–A and 6–B (fig. 3) fluctuated often between two chemical environments. One possible explanation is that episodic variations in freshwater recharge (advection) were superimposed on diffusive flux changes brought about by uplift.

## CONCLUSIONS

Phosphatic concretions, recovered from the Monterey Formation at the Celite mine near Lompoc, Calif., contain vivianite, mitridatite, francolite, and traces of an Mn-Ni-Zn oxide. They occur in finely laminated diatomite, which shows no deformation about the concretions. This structure and the paragenesis of these minerals require that the concretions precipitated under conditions of continuously increasing Eh and pH, after complete compaction of the sediment. On the basis of modern occurrences of vivianite and mitridatite and the difference in composition of the concretionary francolite and associated marine pelletal francolite, precipitation evidently occurred within a fresh-ground-water environment. The dominant source of major-element-oxides and REE's was marine biogenic debris. Our interpretation of this complex chemistry is that the concretions precipitated as a result of the decomposition of marine phases—organic matter, biogenic silica, and $CaCO_3$—during uplift into the phreatic and (or) vadose zones of the terrestrial environment.

## REFERENCES CITED


Altschuler, Z.S., Berman, Sol, and Cuttitta, Frank, 1967, Rare earths in phosphorites—geochemistry and potential recovery, *in* Geological Survey research, 1967: U.S. Geological Survey Professional Paper 575–B, p. B1–B9.

Altschuler, Z.S., 1973, The weathering of phosphate deposits—geochemical and environmental aspects, *in* Griffith, E.J., and others, eds., Environmental phosphorus handbook: New York, Wiley, p. 33–96.

Bramlette, M.N., 1946, The Monterey Formation of California and the origin of its siliceous rocks: U.S. Geological Survey Professional Paper 212, 55 p.

Brumsack, H.J., 1986, The inorganic geochemistry of Cretaceous black shales (DSDP leg 41) in comparison to modern upwelling sediments from the Gulf of California, *in* Summerhayes, C. P., and Shackleton, N.J., eds., North Atlantic paleoceanography: Geological Society of America Special Publication 21, p. 447–462.

Calvert, S.E., 1964, Factors affecting distribution of laminated sediments in the Gulf of California, *in* van Andel, T.H., and Shor, G.G., eds., The marine geology of the Gulf of California: American Association of Petroleum Geologists Memoir 3, p. 311–330.

Carpenter, Roy, 1969, Factors controlling the marine geochemistry of fluorine: Geochimica et Cosmochimica Acta, v. 33, no. 10, p. 1153–1167.

Collier, R.W., and Edmond, John, 1984, The trace element chemistry of marine biogenic particulate matter: Progress in Oceanography, v. 13, no. 2, p. 113–199.

Crock, J.G., and Lichte, F.E., 1982, Determination of rare earth elements in geological materials by inductively coupled argon plasma/atomic emission spectrometry: Analytical Chemistry, v. 54, no. 8, p. 1329–1332.

Dana, E.S., 1935, A textbook of mineralogy (4th ed., revised by W.E. Ford): New York, Wiley, 851 p.

De Baar, H.J.W., Bacon, M.P., Brewer, P.G., and Bruland, K.W., 1985, Rare earth elements in the Pacific and Atlantic Oceans: Geochimica et Cosmochimica Acta, v. 49, no. 9, p. 1943–1959.

Donegan, Dave, and Schrader, Hans, 1981, Modern analogues of the Miocene diatomaceous Monterey Shale of California—evidence from sedimentologic and micropaleontogic study, *in* Garrison, R.E., and Douglas, R.G., eds., The Monterey Formation and related siliceous rocks of California: Society of Economic Paleontologists and Mineralogists, Pacific Section Book 15, p. 149–157.

Elderfield, H., Hawkesworth, C.J., Greaves, M.J., and Calvert, S.E., 1981, Rare earth element geochemistry of oceanic ferromanganese nodules and associated sediments: Geochimica et Cosmochimica Acta, v. 45, no. 4, p. 513–528.

Froelich, P.N., Arthur, M.A., Burnett, W.C., Deakin, M., Hensley, V., Jahnke, R., Kaul, L., Kim, K.H., Roe, K., Soutar, A., and Vathakanon, C., 1988, Early diagenesis of organic matter in Peru continental margin sediments; phosphorite precipitation: Marine Geology, v. 80, no. 3–4, p. 309–343.

Govean, F.M. and Garrison, R.E., 1981, Significance of laminated and massive diatomites in the upper part of the Monterey Formation, California, *in* Garrison, R.E., and Douglas, R.G., eds., The Monterey Formation and related siliceous rocks of

California: Society of Economic Paleontologists and Mineralogists, Pacific Section Book 15, p. 181–198.

Gulbrandsen, R. A., 1970, Relation of carbon dioxide content of apatite of the Phosphoria Formation to regional facies, *in* Geological Survey research, 1970: U.S. Geological Survey Professional Paper 700–B, p. B9–B13.

Hamilton, E.L., 1976, Variations of density and porosity with depth in deep-sea sediments: Journal of Sedimentary Petrology, v. 46, no. 2, p. 280–300.

Haskin, M.A., and Haskin, L.A., 1966, Rare earths in European shale; a redetermination: Science, v. 154, no. 3748, p. 507–509.

Hearn, P.P., Parkhurst, D.L., and Callender, E., 1983, Authigenic vivianite in Potomac River sediments; control by ferric oxyhydroxides: Journal of Sedimentary Petrology, v. 53, no. 1, p. 165–177.

Hem, J.D., Lind, C.J., and Roberson, C.E., 1989, Coprecipitation and redox reactions of manganese oxides with copper and nickel: Geochimica et Cosmochimica Acta, v. 53, no. 11, p. 2811–2822.

Hem, J.D., Roberson, C.E., and Lind, C.J., 1987, Synthesis and stability of hetaerolite, $ZnMn_2O_4$, at 25°C: Geochimica et Cosmochimica Acta, v. 51, no. 6, p. 1539–1547.

Henderson, G.S., Black, P.M., Rodgers, K.A., and Rankin, P.C., 1984, New data on New Zealand vivianite and metavivianite: New Zealand Journal of Geology and Geophysics, v. 27, no. 3, p. 367–378.

Isaacs, C.M., 1980, Diagenesis in the Monterey Formation examined laterally along the coast near Santa Barbara, California: Stanford, Calif., Stanford University, Ph.D. thesis, 329 p.

———1981, Porosity reduction during diagenesis of the Monterey Formation, Santa Barbara coastal area, California, *in* Garrison, R.E. and Douglas R.G., eds., The Monterey Formation and related siliceous rocks of California: Society of Economic Paleontologists and Mineralogists, Pacific Section Book 15, p. 257–271.

———1989, Field trip guide to the Miocene Monterey Formation, Salinas and Santa Barbara areas, California: International Geological Congress, 28th, Washington, D.C., 1989, Field Trip Guidebook, p. 21–50.

Jahnke, R.A., 1984, The synthesis and solubility of carbonate fluorapatite: American Journal of Science, v. 284, no. 1, p. 58–78.

Keller, M.A., and Isaacs, C.M., 1985, An evaluation of temperature scales for silica diagenesis in diatomaceous sequences including a new approach based on the Miocene Monterey Formation: GeoMarine Letters, v. 5, p. 31–35.

Lichte, F.E., Golightly, D.W., and Lamothe, P.J., 1987, Inductively coupled plasma-atomic emission spectoscopy, chap. B *of* Baedecker, P.A., ed., Methods for geochemical analysis: U.S. Geological Survey Bulletin 1770, p. B1–B10.

Littke, R., Klussmann, U., Krooss, B., and Leythaeuser, D., 1991, Quantification of loss of calcite, pyrite, and organic matter due to weathering of Toarcian black shales and effects on kerogen and bitumen characteristics: Geochimica et Cosmochimica Acta, v. 55, no. 11, p. 3369–3378.

Los Angeles County Flood Control District, 1957, Sea-water intrusion in California, app. B *of* California Department of Water Resources, Sea-water intrusion in California: Bulletin 63, 141 p.

Manheim, F.T., Pratt, R.M., and McFarlin, P.F., 1980, Composition and origin of phosphorite deposits on the Blake Plateau, *in* Bentor, Y.K., ed., Marine phosphorites: Society of Economic Paleontologists and Mineralogists Special Publication 29, p. 117–137.

Martin, J.H., and Knauer, G.A., 1973, The elemental composition of plankton: Geochimica et Cosmochimica Acta, v. 37, no. 7, p. 1639–1653.

McArthur, J.M., Benmore, R.A., Coleman, M.L., Soldi, C., Yeh, H.-W., and O'Brien, G.W., 1986, Stable isotopic characteristics of francolite formation: Earth and Planetary Science Letters, v. 77, no. 1, p. 20–34.

McClellan, G.H., 1980, Mineralogy of carbonate fluorapatites: Geological Society of London Journal, v. 137, pt. 6, p. 675–681.

Moore, P.B., 1980, The natural phosphate minerals—crystal chemistry: International Congress on Phosphorus Compounds, 2d, Boston, 1980, Proceedings, p. 105–130.

Murata, K.J., Friedman, Irving, and Madsen, B.M., 1969, Isotopic composition of diagenetic carbonates in marine Miocene formations of California and Oregon: U.S. Geological Survey Professional Paper 614–B, p. B1–B24.

Murata, K.J., Friedman, Irving, and Cremer, Marcelyn, 1972, Geochemistry of diagenetic dolomites in Miocene marine formations of California and Oregon: U.S. Geological Survey Professional Paper 724–C, p. C1–C12.

Namson, Jay, and Davis, T.L., 1990, Late Cenozoic fold and thrust belt of the southern Coast Ranges and Santa Maria Basin, California: American Association of Petroleum Geologists Bulletin, v. 74, no. 4, p. 467–492.

Nathan, Y., and Neilsen, H., 1980, Sulfur isotopes in phosphorites, *in* Bentor, Y.K., ed., Marine phosphorites: Society of Economic Paleontologists and Mineralogists Special Publication 29, p. 73–78.

Nriagu, J.O., 1972, Stability of vivianite and ion-pair formation in the system $Fe_3(PO_4)_2$–$H_3PO_4$–$H_2O$: Geochimica et Cosmochimica Acta, v. 36, no. 4, p. 459–470.

Nriagu, J.O., and Dell, C.I., 1974, Diagenetic formation of iron phosphates in recent lake sediments: American Mineralogist, v. 59, no. 9–10, p. 934–946.

Odermatt, J.R., 1986, Transition element chemistry of organic matter in the Monterey Formation, Union Leroy 51–18 well, Santa Maria Valley field, Santa Barbara Co., California: Los Angeles, University of California, M.S. thesis, 213 p.

Palmer, M.R., 1985, Rare earth elements in foraminifera tests: Earth and Planetary Science Letters, v. 73, no. 2–4, p. 285–298.

Piper, D.Z., Baedecker, P.A., Crock, J.G., Burnett, W.C., and Loebner, B.J., 1988, Rare earth elements in the phosphatic-enriched sediment of the Peru shelf: Marine Geology, v. 80, no. 3–4, p. 269–285.

Piper, D.Z., and Kolodny, Yehoshua, 1988, The stable isotopic composition of a phosphorite deposit, $\delta^{13}C$, $\delta^{34}S$, and $\delta^{18}O$: Deep Sea Research, v. 34, no. 5–6, p. 897–911.

Piper, D.Z., Loebner, B., and Aharon, Paul, 1990, Physical and chemical properties of the phosphate deposit on Nauru, western equatorial Pacific, *in* Burnett, W.C., and Riggs, S.R., eds., Phosphate deposits of the world: Cambridge, U.K., Cambridge University Press, v. 3, p. 177–194.

Pisciotto, K.A., 1981, Review of secondary carbonates in the Monterey Formation, California, *in* Garrison, R.E., and Douglas, R.G., eds., The Monterey Formation and related siliceous rocks of California: Society of Economic Paleontologists and Mineralogists, Pacific Section Book 15, p. 273–284.

Pisciotto, K.A., and Garrison, R.E., 1981, Lithofacies and depositional environments of the Monterey Formation, California, *in* Garrison, R.E., and Douglas, R.G., eds., The Monterey Formation and related siliceous rocks of California: Society of Economic Paleontologists and Mineralogists, Pacific Section Book 15, p. 97–122.

Rosenqvist, I.T., 1970, Formation of vivianite in Holocene clay sediments: Lithos, v. 3, no. 4, p. 327–334.

Schuffert, J.D., Kastner, M., Emanuele, G., and Jahnke, R.A., 1990, Carbonate-ion substitution in francolite—a new equation: Geochimica et Cosmochimica Acta, v. 54, no. 8, p. 2323–2328.

Schultz, L.G., Tourtelot, H.A., Gill, J.R., and Boerngen, J.G., 1980, Composition and properties of the Pierre Shale and equivalent rocks, northern Great Plains region: U.S. Geological Survey Professional Paper 1064–B, p. B1–B114.

Sclater, F.R., Boyle, E., and Edmond, J.M., 1976, On the marine geochemistry of nickel: Earth and Planetary Science Letters, v. 31, no. 1, p. 119–128.

Taggart, J.E., Lindsay, J.R., Scott, B.A., Vivit, D.V., Bartel, A.J., and Stewart, K.C., 1987, Analysis of geologic materials by wavelength-dispersive X-ray fluorescence spectrometry, chap. E *of* Baedecker, P.A., ed., Methods for geochemical analysis: U.S. Geological Survey Bulletin 1770, p. E1–E19.

Tien, P.-L., and Waugh, T.C., 1969, Thermal and x-ray studies of earthy vivianite in Graneros shale (upper Cretaceous), Kansas: American Mineralogist, v. 54, no. 9–10, p. 1355–1362.

Vieillard, P., Tardy, Y., and Nahon, D., 1979, Stability fields of clays and aluminum phosphates; parageneses in lateritic weathering of argillaceous phosphatic sediments: American Mineralogist, v. 64, no. 5–6, p. 626–634.

Wedepohl, K.H., ed., 1969, Handbook of geochemistry: Berlin, Springer-Verlag, 2 v.

Woodring, W.P., and Bramlette, M.N., 1950, Geology and paleontology of the Santa Maria district, California: U.S. Geological Survey Professional Paper 222, 185 p.


U.S. DEPARTMENT OF THE INTERIOR
MARCH 3, 1849